nature photonics

ARTICLES

PUBLISHED ONLINE: 7 NOVEMBER 2016 | DOI: 10.1038/NPHOTON.2016.216

Lasing and anti-lasing in a single cavity

Zi Jing Wong[1†], Ye-Long Xu[1†], Jeongmin Kim[1†], Kevin O'Brien[1], Yuan Wang[1,2], Liang Feng[3*] and Xiang Zhang[1,2,4*]

Lasing, light amplification by stimulated emission of radiation, is a key attribute for many important applications in optical communications, medicine and defence. Conversely, anti-lasing represents the time-reversed counterpart of laser emission, where incoming radiation is coherently absorbed. Here, we experimentally realize lasing and anti-lasing at the same frequency in a single cavity using parity–time symmetry. Because of the time-reversal property, the demonstrated lasing and anti-lasing resonances share common resonant features such as identical frequency dependence, coherent in-phase response and fine spectral resolution. Lasing and anti-lasing in a single device offers a new route for light modulation with high contrast approaching the ultimate limit.

Loss of optical power by material absorption is a serious problem in optics, significantly degrading the performance and efficiency of optical devices such as microscopes and fibre networks. Oppositely, optical gain media have enabled light amplification that overcomes the undesirable absorption[1,2], leading to the birth of lasers. A laser distinguishes itself from other light sources by its intrinsic coherence in both space and time. The time-reversed counterpart of laser emission enables coherent perfect absorption in a loss-dominant resonator, facilitating the emergence of anti-lasers. An anti-laser, or coherent perfect absorber (CPA), based on interferometric control of absorption is known to completely annihilate both the transmitted and reflected light signals[3,4], with promising novel applications in enhanced nano-optical mode coupling[5], ultrathin perfect absorbers[6,7] and integrated photonic circuits[8]. While both the laser and anti-laser are individually important functions to advance photonics technology, lasing and anti-lasing in a single cavity (that is, a CPA–laser) is counterintuitive since conventional optical physics requires either gain or loss, respectively, but not both. Despite the difficulty in attaining lasing and anti-lasing resonances that coexist, its realization can directly lead to a multifunctional optical device with the capabilities of a laser, an amplifier, a modulator and an absorber. Within the same cavity, lasing and anti-lasing can be engineered to not suppress each other but instead coexist to offer an unprecedented control over coherent amplification and absorption. For example, in the modulator community, a key figure-of-merit to assess the performance of optical modulators is the modulation depth, and significant challenges remain to effectively approach the ultimate modulation depth set by the maximum contrast between the lasing and anti-lasing states[9,10]. While many light modulation and switching schemes have been proposed relying on either linear or nonlinear light controls[11–15], the state-of-the-art modulation depth is still orders of magnitude lower than the ultimate limit attainable with the lasing and anti-lasing resonances.

Parity–time symmetry

The CPA–laser concept was first proposed theoretically in 2010[9], showing the possibility to realize both lasing and anti-lasing in a single optical system of parity–time ($\mathcal{PT}$) symmetry[16,17]. $\mathcal{PT}$ symmetry in optics requires the real part of refractive index modulation to be symmetric $n'(x) = n'(-x)$, and the imaginary part of the index to be anti-symmetric $n''(x) = -n''(-x)$. In recent years, meticulous design of the real and imaginary part of the refractive index has led to many unique optical properties such as optical phase transition from $\mathcal{PT}$-symmetric phase to broken phase[18–23] and unidirectional light transport[24–26]. $\mathcal{PT}$ symmetry essentially offers a new strategy to utilize loss to control gain and its associated optical properties in the $\mathcal{PT}$-broken phase, deliberately manipulating the resonant modes in laser cavities[27,28] and broadening the physics and capabilities of the lasers[29–31]. A $\mathcal{PT}$-symmetric structure composed of two homogenous gain and loss regions embedded under a uniform index grating was theoretically suggested for realizing a CPA–laser[9]. Follow-up studies used the scattering matrix formalism[32] and later a two-dimensional $\mathcal{PT}$-symmetric ring cavity structure was then proposed[10]. Here, we experimentally demonstrate lasing and anti-lasing in a single cavity by designing a distributed feedback structure with pure gain–loss and balanced $\mathcal{PT}$ modulation in each unit cell along the light propagation direction. The gain and loss and the cavity are carefully engineered to approach the ultimate light control limit by interferometrically switching photons between the lasing and anti-lasing states. $\mathcal{PT}$ symmetry ensures that the two opposing states occur at the same frequency with balanced amplification and absorption magnitude. The optical feedback in the CPA–laser cavity can thus support both lasing and anti-lasing modes with complex conjugate gain and loss coefficients. These two eigenmodes are spatially shifted by half the Bragg wavelength, with an offset of π in phase. The phase offset between the incoming coherent light beams shifts the constructive interference pattern from one to the other, showing a large modulation contrast between the coherent lasing and anti-lasing modes.

Design

The CPA–laser is designed using a straight waveguide of 500-nm-thick InGaAsP multiple quantum wells (MQWs) as a gain medium on an InP substrate. The alternating $\mathcal{PT}$-symmetric gain–loss modulation is introduced by periodically placing thin absorbing Cr/Ge structures on top of the waveguide (Fig. 1). To strongly confine light in the InGaAsP MQWs for maximum modal gain, the waveguide is designed to be 1.5-μm-wide and extend 1 μm deep into the InP substrate. When the pump light supplies a

[1]NSF Nanoscale Science and Engineering Center, 3112 Etcheverry Hall, University of California, Berkeley, California 94720, USA. [2]Materials Sciences Division, Lawrence Berkeley National Laboratory, 1 Cyclotron Road, Berkeley, California 94720, USA. [3]Department of Electrical Engineering, The State University of New York at Buffalo, Buffalo, New York 14260, USA. [4]Department of Physics, King Abdulaziz University, Jeddah 21589, Saudi Arabia. †These authors contributed equally to this work. *e-mail: xiang@berkeley.edu; fengl@buffalo.edu

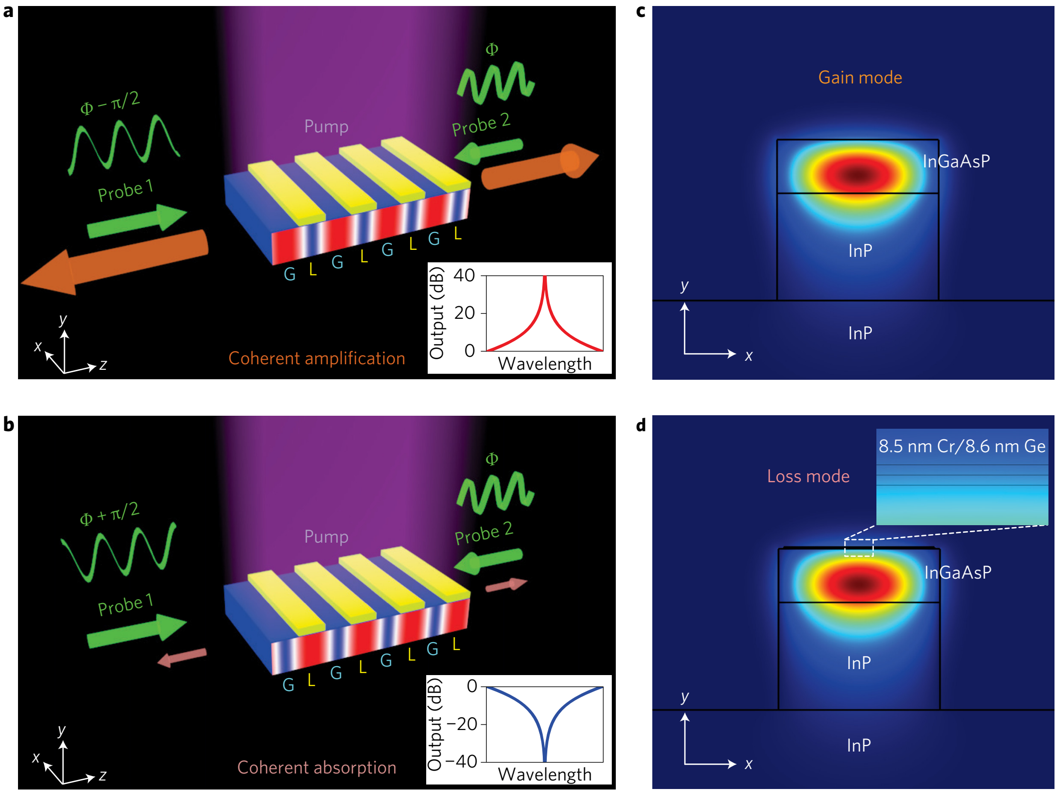

Figure 1 | CPA–laser for lasing and anti-lasing in a single cavity. a,b, Schematics showing the principle of the CPA–laser, where the pure gain (G)–loss (L) $\mathcal{PT}$ modulation is introduced by placing periodic loss structures on a semiconductor InGaAsP/InP gain waveguide. The period of the $\mathcal{PT}$ modulation is designed to be half of the effective wavelength of guided light, corresponding to the Bragg resonant condition. By uniformly pumping the device, the balanced gain–loss $\mathcal{PT}$-symmetry condition is satisfied to attain both lasing and anti-lasing eigenmodes within the same cavity. The coherent interferometric phase control on the guided light incoming from both directions can selectively excite either the lasing or the anti-lasing mode. **a**, When the incoming probe beams are $-\pi/2$ offset in phase, the Bragg resonant electric fields constructively interfere only in the gain regions, which leads to strongly amplified outgoing waves and a sharp peak in the output spectrum corresponding to the lasing mode. **b**, When the incoming probe beams are $\pi/2$ offset in phase, the device falls in the anti-lasing mode, where the Bragg interference of electric fields is strongly confined only in the loss regions, causing strong absorption and a narrow dip in the output spectrum. **c**, Cross-sectional eigenfield distribution of the lasing or amplification mode, leading to a gain-dominant effective index of $n_{\text{eff}} = 3.205 - 0.003i$. **d**, Introducing the 8.5 nm Cr/8.6 nm Ge structures on top of the gain waveguide results in a similar cross-sectional eigenfield distribution for the anti-lasing or absorption mode with a loss-dominant effective index of $n_{\text{eff}} = 3.205 + 0.003i$. These complex conjugate effective indices lead to the pure gain–loss $\mathcal{PT}$ modulation required to support both lasing and anti-lasing modes in the CPA–laser cavity.

considerable gain to the InGaAsP/InP waveguide, the loss of the Cr/Ge structures reverses the sign of the imaginary part of the local modal index while maintaining the same real part and similar cross-sectional eigenfield distribution along the device. In our design, the Cr/Ge structures consist of 8.5-nm-thick Cr and 8.6-nm-thick Ge, which lead to effective modal indices for both the loss and gain regions of $n_{\text{eff}} = 3.205 \pm 0.003i$, respectively, at the wavelength around 1,556 nm. As a result, the guided light experiences an effectively pure gain–loss $\mathcal{PT}$-symmetric modulation as:

$$\Delta n = \begin{cases} n_{\text{gain}} = -in'' & (0 < z < a/2) \\ n_{\text{loss}} = in'' & (a/2 < z < a) \end{cases}$$

where n'' denotes the index modulation in only the imaginary part, z is the distance along the light propagation direction and a is the Bragg period corresponding to half of the effective wavelength of the guided light. While the gain–loss modulation results in distributed optical feedback similar to conventional loss-coupled distributed feedback lasers[33], only the optical modulation stringently satisfying the $\mathcal{PT}$ symmetry can sustain both lasing and anti-lasing at the same eigenfrequency in a single compact device[9]. In our work, the lasing and anti-lasing eigenmodes are degenerate at the boundary of the Brillouin zone due to the distributed Bragg feedback introduced by the periodic gain–loss modulation. By carefully designing the optical transfer matrix $M = [M_{11}\ M_{12};\ M_{21}\ M_{22}]$ of the two-port system using the coupled mode theory, our CPA–laser can uniquely satisfy both the lasing ($M_{22} = 0$) and anti-lasing ($M_{11} = 0$) conditions (see Supplementary Information), and approach the CPA–laser point[9,32]. Remarkably, the realization of $\mathcal{PT}$-broken phase creates two mutually exclusive states, that is, lasing (amplification) and anti-lasing (absorption) modes at the same frequency in the same device for the guided light. As shown in Fig. 1a, b, respectively, the lasing and anti-lasing eigenstates are orthogonal and spatially shifted by π in phase. Therefore, optical switching between these two states can be demonstrated by tuning the initial phase offset of two counter-propagating incoming beams to locate the constructive interference on-demand. When the two incoming probe beams are $-\pi/2$ offset in phase (Fig. 1a), light is interferometrically confined in the gain regions where stimulated emission from the lasing mode takes place to resonantly amplify the outgoing beams. Similarly, the same lasing mode can lead to lasing emission without any probe beam. When the two incoming probe beams are of a $\pi/2$ phase offset (Fig. 1b), light becomes localized in the loss regions and coherently absorbed by the anti-lasing mode, thus strongly attenuating and even fully annihilating the outgoing beams. Therefore, one can envision building an optical amplitude modulator with an extremely large modulation depth, whereby switching the phase of the second probe beam (as a control signal),

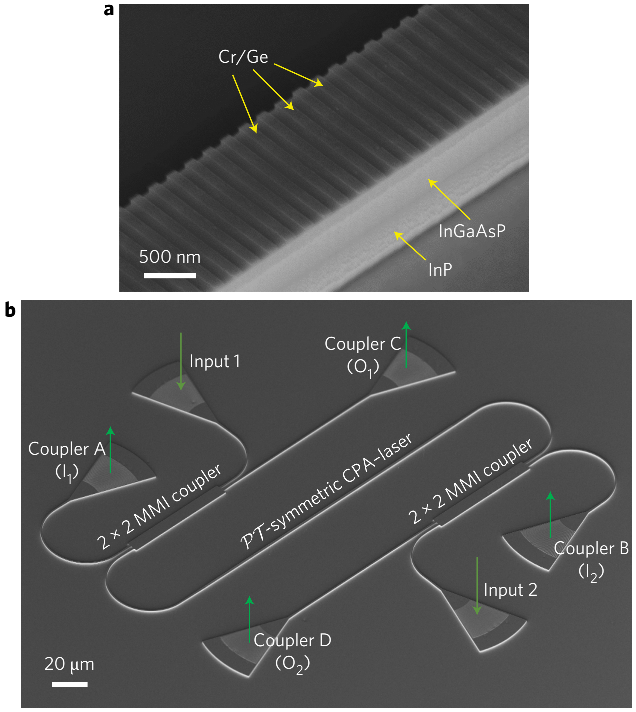

Figure 2 | Experimental characterization scheme for the CPA–laser. **a**, SEM image of the fabricated CPA–laser on the InGaAsP/InP platform. The guided coherent probe beams coming from both directions selectively excite either the lasing mode or the anti-lasing mode via interferometric phase control. **b**, Full device layout to measure the incoming and outgoing light passing through the CPA–laser to characterize the amplification by the lasing mode and the absorption due to the anti-lasing mode. Two probe beams are coupled into the waveguide using input 1 and input 2 grating couplers, respectively. Each of them is then equally split into two paths by a 2 × 2 multimode interference (MMI) coupler to isolate the input and output signals. By collecting the signal at coupler A and coupler B, the intensity of input light waves at both boundaries of the CPA–laser can be determined; meanwhile, upon interacting with the CPA–laser, the outgoing waves are collected by coupler C and coupler D. The output coefficient of the CPA–laser can thus be obtained by monitoring the outgoing light waves from these grating couplers as $\Theta = 2((O_1 + O_2)/(I_1 + I_2))$, which is used to characterize the corresponding amplification and absorption of the fabricated CPA–laser.

the output intensity of the first probe beam (that is, the signal) can be either strongly amplified or terminated. To minimize the possible scattering due to mode mismatch when switching between these two modes, the lasing and anti-lasing modes are designed to have similar cross-sectional electric field distribution confined in the InGaAsP MQWs gain layer (Fig. 1c,d).

Fabrication and measurement

The CPA–laser sample was fabricated using overlay electron-beam lithography (see Supplementary Information) and a scanning electron microscope (SEM) image of it is shown in Fig. 2a. In experiments, it is necessary to separate the input and output signals and measure both the transmission and reflection spectra of the CPA–laser. Although such a measurement is easy to perform for free-space devices[4], to isolate the output signal from the input on a chip would require the use of external components that can route the light. To address this challenge in our on-chip measurement, we intentionally designed and fabricated, together with the CPA–laser, 6 groups of Ge grating couplers and a pair of 2 × 2 multimode interference (MMI) couplers, as shown in Fig. 2b. While two input grating couplers convert light from free space to the guided mode, two MMI couplers efficiently sort the output signal from the input and guide them to different grating couplers that radiate the guided light back to free space. Essentially, the input beams (I_1 and I_2) entering the CPA–laser are monitored using coupler A and coupler B, respectively, while the outgoing beams (O_1 and O_2) upon resonant amplification or absorption are collected using coupler C and coupler D, respectively. The output coefficient Θ of the CPA–laser, defined as the ratio of total outgoing light intensity to the total incoming light intensity for the device, can therefore be determined:

$$\Theta = 2\left(\frac{O_1 + O_2}{I_1 + I_2}\right)$$

Note that the probing and switching of the lasing and anti-lasing modes to observe coherent amplification and absorption are based on a linear interferometric strategy on the probe beams and are thus insensitive to the pump-induced background emission. Therefore, the undesired noise contribution is deducted in all the terms defined in Θ (see Supplementary Information for more details).

Experimental results

For a CPA–laser operating in the $\mathcal{PT}$-broken phase, the existence of the lasing mode can be directly validated with the lasing emission alone without the two probe beams. The $\mathcal{PT}$ gain–loss modulation was obtained by uniformly pumping the entire length of the CPA–laser (see Supplementary Information), which produced the Bragg optical feedback to support the mode oscillation. As the pumping energy density is increased above the lasing threshold, stimulated emission of the resonant lasing mode dominates and lasing action is observed. As shown in Fig. 3a, at the pump energy density of 4.2 μJ cm^{-2}, a distinct lasing peak occurs, which corresponds to the resonant lasing mode associated with the $\mathcal{PT}$-broken phase. The output light intensity as a function of pump energy density is plotted in Fig. 3b, which shows the lasing threshold, that is, the nonlinear kink, at around 3.6 μJ cm^{-2}. On the other hand, the anti-lasing mode for coherent perfect absorption must be characterized using two coherent probe beams with the pump constantly on. While it is ideal to have a strong pump to enhance lasing emission, the nonlinear laser dynamics above the lasing threshold might alter the $\mathcal{PT}$-symmetry condition[9] required for simultaneous lasing and anti-lasing resonance (see Supplementary Information). Therefore, we intentionally fixed the pump around the lasing threshold at 3.6 μJ cm^{-2}, where the high-power-associated optical nonlinearities were negligible, when we conducted the anti-lasing measurements. By controlling the phase offset between two probe beams to be $\pi/2$, we successfully excited the anti-lasing eigenmode with constructive light interference mainly localized in the loss regions. As shown in Fig. 3c, a sharp absorption dip of Θ down to −15 dB can be observed at the anti-lasing resonant wavelength around 1,555.8 nm. Meanwhile, when the phase offset between two probe beams was switched to $-\pi/2$, under the same pumping condition, it was the lasing mode that was being resonantly excited, with a maximum amplified Θ of 15 dB at the same wavelength (see Supplementary Information for the theoretical analysis and the detailed measurements with error bars to verify the reliability of our data). Our results clearly demonstrate coherent amplification and absorption with symmetric amplitudes at the same wavelength, confirming the coexistence of lasing and anti-lasing modes in the CPA–laser using the concept of $\mathcal{PT}$ symmetry. In contrast to standard optical modulators and amplifiers that are typically limited to either absorption or amplification alone, our CPA–laser achieves both coherent amplification and coherent absorption within a single device. Its unique ability to switch between lasing and anti-lasing states simply by tuning the phase renders it promising to approach the ultimate limit of modulation depth. As our device operates close to the singular

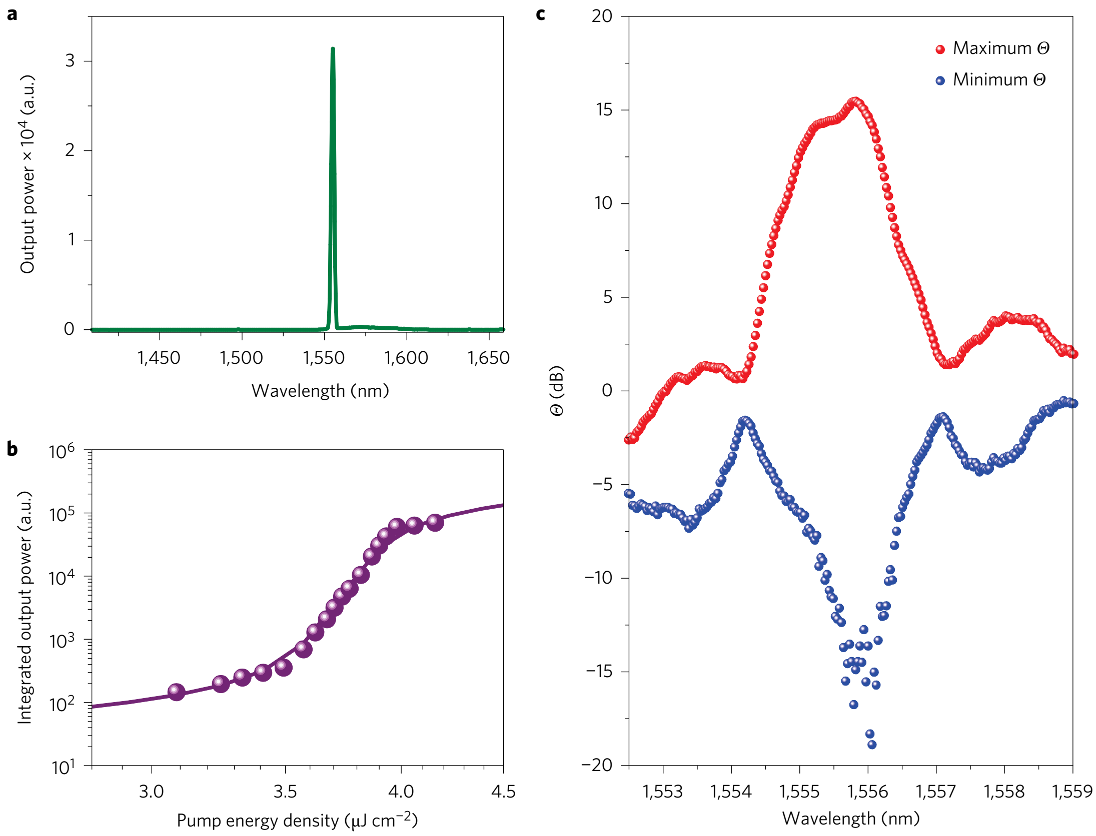

Figure 3 | Lasing and anti-lasing measurement. a, The lasing spectrum at the pump energy density of 4.2 μJ cm^{-2}, above the lasing threshold, showing a distinct single-mode lasing resonance. **b**, Light–light curve plotted on a log–log scale, where the data points represent the experimental values and the solid line is based on the best fit of the rate equation model. The lasing threshold occurs at around 3.6 μJ cm^{-2}, above which the effect of nonlinear laser dynamics on the $\mathcal{PT}$ symmetry and properties of the CPA–laser remains unclear. We therefore performed the lasing and anti-lasing characterizations around the lasing threshold. **c**, The spectra output coefficient $\Theta = 2((O_1 + O_2)/(I_1 + I_2))$ of the CPA–laser in the wavelength range from 1,552.5 nm to 1,559 nm for the pump energy density of 3.6 μJ cm^{-2} at the lasing threshold. At 1,555.8 nm, with the $-\pi/2$ phase-offset probe beams, the maximum Θ (red), manifests a distinct amplification peak of 15 dB, corresponding to the resonant lasing mode; while with the $\pi/2$ phase-offset probe beams, the minimum Θ (blue), is associated with the anti-lasing mode inducing an absorption dip down to –15 dB. This essentially confirms that coherent amplification and absorption can be attained in a single lasing cavity. The lasing and anti-lasing modes share similar resonant wavelengths, and have symmetric amplification and absorption magnitude, all due to the complex conjugate effective indices supported by the $\mathcal{PT}$-broken phase.

CPA–laser point, a large extinction ratio of 30 dB is experimentally obtained. It is important to note that strong probe beams can cause gain saturation and nonlinear frequency mixing with the pump beams. This in principle can perturb the $\mathcal{PT}$-symmetry condition and degrade the associated amplification and absorption performance. By measuring the output light intensity for different incoming probe powers, we showed that the average probe power used fell within the linear response regime (see Supplementary Information). This power scaling result proves that the sharp amplification and absorption effect observed in our CPA–laser strictly follows the linear scattering theory and it eliminates any contribution from gain saturation and other nonlinear properties.

While it is evident that the light control in our CPA–laser is a linear process based on the coherent tuning of the optical phase, we further investigated the related phase sensitivity at different wavelengths by monitoring the outgoing waves (Fig. 4a,b). The maps of electric field amplitude distribution both inside and outside the CPA–laser device for different wavelengths and phase offset conditions are shown in Fig. 4c. At 1,555.8 nm, the system is on resonance where the strong distributed Bragg feedback is dominant, either the lasing (phase offset $\Delta\phi = -\pi/2$) or anti-lasing (phase offset $\Delta\phi = \pi/2$) mode is excited with the constructive interference in the gain or loss regions, respectively. This requires the electric field inside the CPA–laser to be closely in-phase, leading to synchronized outgoing waves from two different ports of the device. This in-phase behaviour is almost identical for both the lasing and anti-lasing modes, which again confirms the attainment of the lasing and anti-lasing modes in a single cavity by $\mathcal{PT}$ symmetry. In the CPA mode, almost all of the incoming photons of probe beams are absorbed by the lossy Cr/Ge structures. When the operation wavelength is off resonance, a weak optical feedback is formed. Outgoing waves from the two ports continuously vary between in-phase and out-of-phase in wavelengths as evidenced by the side ripples in the output coefficient spectra (Fig. 3c). The system becomes almost phase-insensitive when the amplification and absorption spectra cross[4], for example, at the wavelength of 1,554.2 nm. Here, the electric field amplitude is equally distributed between the gain and loss regions, while the outgoing waves are completely out-of-phase, equal to the scattered field from incoherent illumination. Measurement of the output phase difference between the two ports as a function of wavelength indeed showed that the output phase difference gradually diminished as it approached the coherent amplification and absorption wavelength (see Supplementary Information). This further proves the same in-phase response of the lasing and anti-lasing modes in the CPA–laser. Hence, the introduced $\mathcal{PT}$-broken phase facilitates the identical resonant nature for these two opposite modes and thus enables coherent amplification and absorption switching towards the ultimate contrast limit.

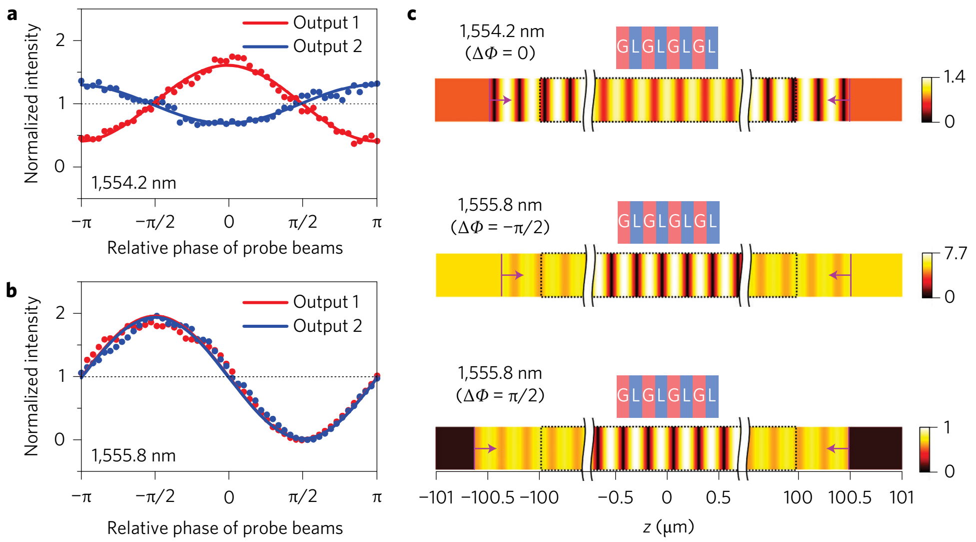

Figure 4 | Phase response of outgoing waves by coherent light control. a,b, The measured phase response from both the normalized output 1 and output 2 signals by continuously varying the phase offset between probe beams from $-\pi$ to π for 1,554.2 nm (**a**) and 1,555.8 nm (**b**) wavelengths. **c**, Simulation results showing the electric field amplitude (colour scale bars) distribution inside and outside the structure for different wavelengths and relative phase ($\Delta\phi$) conditions between the input probe beams. The dotted lines mark the position of the CPA–laser with the arrows representing the incoming probe beams. Depending on the arrow position, a phase shift to one of the incident probe beams can be introduced. For the phase-insensitive wavelength at 1,554.2 nm (as a control), the two outgoing waves are completely out-of-phase. The interference pattern is thus located between the gain and loss regions, leading to scattered intensities similar to incoherent illumination. When the resonant mode is excited, however, the field inside the CPA–laser results in constructive interference, such that the outgoing waves become in-phase. Therefore, the lasing and anti-lasing modes can both be supported inside the CPA–laser for the designed Bragg resonant wavelength at 1,555.8 nm. When the probe beams are $-\pi/2$ offset in phase, the interfered electric fields are predominantly confined in the gain regions, which leads to a strong coherent amplification; while a $\pi/2$ offset in phase will cause a sharp coherent absorption due to the confinement of electric field in the loss regions. The results confirm that the two outgoing waves are out-of-phase for the phase-insensitive wavelength; while as the operation wavelength approaches the lasing and anti-lasing resonance, the two outgoing waves become closely in-phase due to the constructively interfering excitation of the resonant mode inside the CPA–laser. G, gain; L, loss.

Conclusion

Our demonstration of the CPA–laser provides an effective route of light manipulation and control through the interplay between material gain and loss by $\mathcal{PT}$ symmetry. In the $\mathcal{PT}$-broken phase, we realized for the first time both lasing and anti-lasing: by controlling the relative phase offset of the input signals, either coherent amplification or absorption could be obtained within a single device. The switchable lasing and anti-lasing modes achieved here enables a highly efficient coherent control strategy with an excellent amplification-to-absorption contrast. In practice, this contrast is mainly limited by how close the system approaches the singular CPA–laser point (see Supplementary Information). Although nonlinearities associated with lasing may potentially alter the $\mathcal{PT}$-symmetry condition in our current design, a theory incorporating optical nonlinearity[34] for $\mathcal{PT}$ symmetry can be developed in the future. From the device perspective, the demonstrated CPA–laser can operate as a laser, an amplifier, a modulator and an absorber, essentially encompassing many useful on-chip optical functions. Such a versatile device has great potential to be a general building block for next-generation photonic integrated circuits, significantly reducing the integration complexity while realizing multifunctional operations for efficient information processing in optical communications.

Received 19 February 2016; accepted 5 October 2016;
published online 7 November 2016

References

1. Xiao, S. *et al.* Loss-free and active optical negative-index metamaterials. *Nature* **466,** 735–738 (2010).
2. Nezhad, M. P. *et al.* Room-temperature subwavelength metallo-dielectric lasers. *Nat. Photon.* **4,** 395–399 (2010).
3. Chong, Y. D., Ge, L., Cao, H. & Stone, A. D. Coherent perfect absorbers: time-reversed lasers. *Phys. Rev. Lett.* **105,** 053901 (2010).
4. Wan, W. *et al.* Time-reversed lasing and interferometric control of absorption. *Science* **331,** 889–892 (2011).
5. Noh, H., Chong, Y., Stone, A. D. & Cao, H. Perfect coupling of light to surface plasmons by coherent absorption. *Phys. Rev. Lett.* **108,** 186805 (2012).
6. Pu, M. *et al.* Ultrathin broadband nearly perfect absorber with symmetrical coherent illumination. *Opt. Express* **20,** 2246–2254 (2012).
7. Fan, Y., Zhang, F., Zhao, Q., Wei, Z. & Li, H. Tunable terahertz coherent perfect absorption in a monolayer graphene. *Opt. Lett.* **39,** 6269–6272 (2014).
8. Bruck, R. & Muskens, O. L. Plasmonic nanoantennas as integrated coherent perfect absorbers on SOI waveguides for modulators and all-optical switches. *Opt. Express* **21,** 27652–27661 (2013).
9. Longhi, S. $\mathcal{PT}$-symmetric laser absorber. *Phys. Rev. A* **82,** 031801(R) (2010).
10. Longhi, S. & Feng, L. $\mathcal{PT}$-symmetric microring laser-absorber. *Opt. Lett.* **39,** 5026–5029 (2014).
11. Reed, G. T., Mashanovich, G., Gardes, F. Y. & Thomson, D. J. Silicon optical modulators. *Nat. Photon.* **4,** 518–526 (2010).
12. Zhang, J., MacDonald, K. F. & Zheludev, N. I. Controlling light-with-light without nonlinearity. *Light Sci. Appl.* **1,** e18 (2012).
13. Xu, Q., Schmidt, B., Pradhan, S. & Lipson, M. Micrometre-scale silicon electro-optic modulator. *Nature* **435,** 325–327 (2005).
14. Hochberg, M. *et al.* Terahertz all-optical modulation in a silicon-polymer hybrid system. *Nat. Mater.* **5,** 703–709 (2006).
15. Schackert, F., Roy, A., Hatridge, M., Devoret, M. H. & Stone, A. D. Three-wave mixing with three incoming waves: signal-idler coherent attenuation and gain enhancement in a parametric amplifier. *Phys. Rev. Lett.* **111,** 073903 (2013).
16. Bender, C. M. & Böttcher, S. Real spectra in non-Hermitian Hamiltonians having $\mathcal{PT}$ symmetry. *Phys. Rev. Lett.* **80,** 5243–5246 (1998).
17. Bender, C. M. Making sense of non-Hermitian Hamiltonians. *Rep. Prog. Phys.* **70,** 947–1018 (2007).
18. Makris, K. G., El-Ganainy, R., Christodoulides, D. N. & Musslimani, Z. H. Beam dynamics in $\mathcal{PT}$-symmetric optical lattices. *Phys. Rev. Lett.* **100,** 103904 (2008).
19. Klaiman, S., Guenther, U. & Moiseyev, N. Visualization of branch points in $\mathcal{PT}$symmetric waveguides. *Phys. Rev. Lett.* **101,** 080402 (2008).
20. Longhi, S. Bloch oscillations in complex crystals with $\mathcal{PT}$ symmetry. *Phys. Rev. Lett.* **103,** 123601 (2009).

21. Rüter, C. E. *et al*. Observation of parity–time symmetry in optics. *Nat. Phys.* **6,** 192–195 (2010).
22. Regensburger, A. *et al*. Parity–time synthetic photonic lattices. *Nature* **488,** 167–171 (2012).
23. Baum, B., Alaeian, H. & Dionne, J. A parity-time symmetric coherent plasmonic absorber-amplifier. *J. Appl. Phys.* **117,** 063106 (2015).
24. Lin, Z. *et al*. Unidirectional invisibility induced by $\mathcal{PT}$-symmetric periodic structures. *Phys. Rev. Lett.* **106,** 213901 (2011).
25. Feng, L. *et al*. Experimental demonstration of a unidirectional reflectionless parity–time metamaterial at optical frequencies. *Nat. Mater.* **12,** 108–113 (2013).
26. Peng, B. *et al*. Parity–time-symmetric whispering-gallery microcavities. *Nat. Phys.* **10,** 394–398 (2014).
27. Feng, L., Wong, Z. J., Ma, R.-M., Wang, Y. & Zhang, X. Single-mode laser by parity-time symmetry breaking. *Science* **346,** 972–975 (2014).
28. Hodaei, H., Miri, M.-A., Heinrich, M., Christodoulides, D. N. & Khajavikhan, M. Parity-time-symmetric microring lasers. *Science* **346,** 975–978 (2014).
29. Brandstetter *et al*. Reversing the pump dependence of a laser at an exceptional point. *Nat. Commun.* **5,** 4034 (2014).
30. Peng, B. *et al*. Loss-induced suppression and revival of lasing. *Science* **346,** 328–332 (2014).
31. Schomerus, P. Quantum noise and self-sustained radiation of $\mathcal{PT}$-symmetric systems. *Phys. Rev. Lett.* **104,** 233061 (2010).
32. Chong, Y. D., Ge, L. & Stone, A. D. $\mathcal{PT}$-symmetry breaking and laser-absorber modes in optical scattering systems. *Phys. Rev. Lett.* **106,** 093902 (2011).
33. Ghafouri-Shiraz, H. *Distributed Feedback Laser Diodes and Optical Tunable Filters* (Wiley, 2003).
34. Türeci, H. E., Stone, A. D., Ge, L., Rotter, S. & Tandy, R. J. *Ab initio* self-consistent laser theory and random lasers. *Nonlinearity* **22,** C1–C18 (2009).

Acknowledgements

This work was primarily funded by the Director, Office of Science, Office of Basic Energy Sciences, Materials Sciences and Engineering Division of the US Department of Energy within the Metamaterials Program (KC12XZ). L.F. acknowledges the US Army Research Office (W911NF-15-1-0152) that supports the simulation. We thank the Molecular Foundry, Lawrence Berkeley National Laboratory for the technical support in nanofabrication, and D. Olynick for discussions.

Author contributions

Z.J.W., L.F. and X.Z. designed the experiment. Y.-L.X., Z.J.W. and L.F. performed the theoretical calculations and numerical simulations. Z.J.W. fabricated the samples. J.K., Y.-L.X., Z.J.W. and K.O.B. built the optical set-up, Z.J.W., Y.-L.X. and J.K. carried out the measurements and data analysis. All authors contributed to discussions and writing of the manuscript. X.Z., L.F. and Y.W. guided the research.

Additional information

Supplementary information is available in the online version of the paper. Reprints and permissions information is available online at www.nature.com/reprints. Correspondence and requests for materials should be addressed to X.Z. and L.F.

Competing financial interests

The authors declare no competing financial interests.